J Clust Sci (2017) 28:1937–1954
DOI 10.1007/s10876-017-1190-4

ORIGINAL PAPER

Microwave and UV Assisted Methods for Obtaining Novel Composites Based on Fe_2O_3 with Embedded Gold Nanoparticles

J. Pulit-Prociak[1] · J. Chwastowski[1] · M. Banach[1]

Received: 5 December 2016 / Published online: 15 March 2017

Abstract Metallic nanoparticles embedded into the structure of metal oxides may play a role of catalytic substances. Such composites are mostly applied in oxidation reactions. The paper presents two one-step-methods for obtaining nanocomposites of gold embedded in the structure of iron oxide matrices (nanoAu/Fe_2O_3). Gold nanoparticles were formed in situ in the process of iron hydroxide dehydration. Thanks to the use of tannic acid it was possible to effectively reduce gold ions and stabilize the forming metal nanoparticles. The composites were prepared in the fields of microwave, ultraviolet radiation. The physicochemical properties of products were determined by scanning electron microscopy, energy-dispersive X-ray spectroscopy, Fourier transform infrared spectroscopy, X-ray analysis and high-resolution transmission electron microscopy technique with EDS and elemental mapping mode. Also, the catalytic activity of the nanocomposites obtained was evaluated based on the process of methyl orange degradation. It was observed that products obtained according to the microwave radiation method are characterized by improved applying properties.

Keywords Nanogold · Iron oxide · Catalytic activity · Green chemistry

Introduction

The literature provides a number of reports on obtaining of metal/metal oxide composites. They have a great importance in catalysis industry. The literature discloses a number of studies on the reaction of the selective oxidation of benzyl

✉ J. Pulit-Prociak
jolantapulit@chemia.pk.edu.pl

[1] Faculty of Chemical Engineering and Technology, Institute of Chemistry and Inorganic Technology, Cracow University of Technology, Warszawska 24, 31-155 Cracow, Poland

alcohol to benzaldehyde in the presence of catalysts such as Au/U_3O_8 [1], Pd–Ag/pumice [2], Ru–Co–Al/hydrotalcite [3], Ni–Al/hydrotalcite [4]. Currently, the catalytic oxidation of carbon monoxide to carbon dioxide is carried out with the assistance of a catalyst such as noble metals. For this purpose platinum or gold are used [5, 6]. However, the cost of these catalysts means that their use in the oxidation of CO to CO_2 is uneconomical. The literature also describes the use of other, less expensive catalysts. Nanostructured materials which, due to the increased ratio of specific surface area to volume have enhanced chemical activity, are also applied as catalytic materials [7]. Nanoparticles of iron oxide (III) are one of the most frequently used catalysts in the oxidation of CO to CO_2 [8]. Perkas et al. conducted a cyclohexane oxidation process by using the nanoparticles received by sonochemical deposition of metal oxides onto a mesoporous carrier. They demonstrated that the oxidation of cyclohexane can be effectively performed on the surface of iron oxide nanoparticles embedded in mesoporous titanium oxide [9].

Hematite (α-Fe_2O_3) is a low expensive, stable and environment friendly compound which us widely used in catalysis [10], pigments industry [11], lithium ions batteries [12] and gas sensors [13]. Iron oxide may be prepared in the course of vacuum pyrolysis or sol-gel [14] and hydrothermal methods [15]. Beneficial properties of iron oxide nanoparticles have been reported. Also, metallic oxides with embedded metallic nanoparticles are characterized by a wide interest. Their high catalytic activity has been reported in the scientific literature (Au/TiO_2 [16], Au/Mn_2O_3 [17] or Au/ZnO [18]).

The literature provides numerous data on obtaining Au–Fe_2O_3 nanocomposites. Such a composite may be as in catalytic purposes as well. The group of obtaining methods includes deposition-precipitation method [19, 20] or coprecipitation [21].

From both the practical and scientific points of view, it is highly desirable to develop new, easy-to-use catalysts that enable the efficient and selective conducting of the oxidation reaction. It is also important that the properties of the used catalysts do not endanger human health or the environment. This work has been undertaken for this purpose. The aim of this work was to develop a new catalyst based on gold nanoparticles deposited on iron oxide (III). These can be used in the above processes of oxidation. The aim of the study was the comparison of two methods for the preparation of such nanocomposites.

Materials and Methods

Materials

The following compounds were used in this study: iron(III) nitrate nonahydrate ($\geq$99.999%), sodium hydroxide ($\geq$98.0%), gold(III) chloride hydrate ($\geq$99.999%) and tannic acid (p.a.). In catalytic activity tests the following compounds were used: methyl orange (Reag. Ph. Eur.) and sodium borohydride ($\geq$96.0%). All compounds were provided by Sigma Aldrich, Germany.

Methods

Embedding Gold Nanoparticles in the Structure of Iron Oxide

Figure 1 presents the schematic diagram of the performed studies. The first phase was common for both types of process. It concerned the precipitation of iron hydroxide by adding 1.25 cm^3 of sodium hydroxide aqueous solution at a concentration of 15.03 mol/dm^3 to 12.5 cm^3 of iron nitrate aqueous solution at a

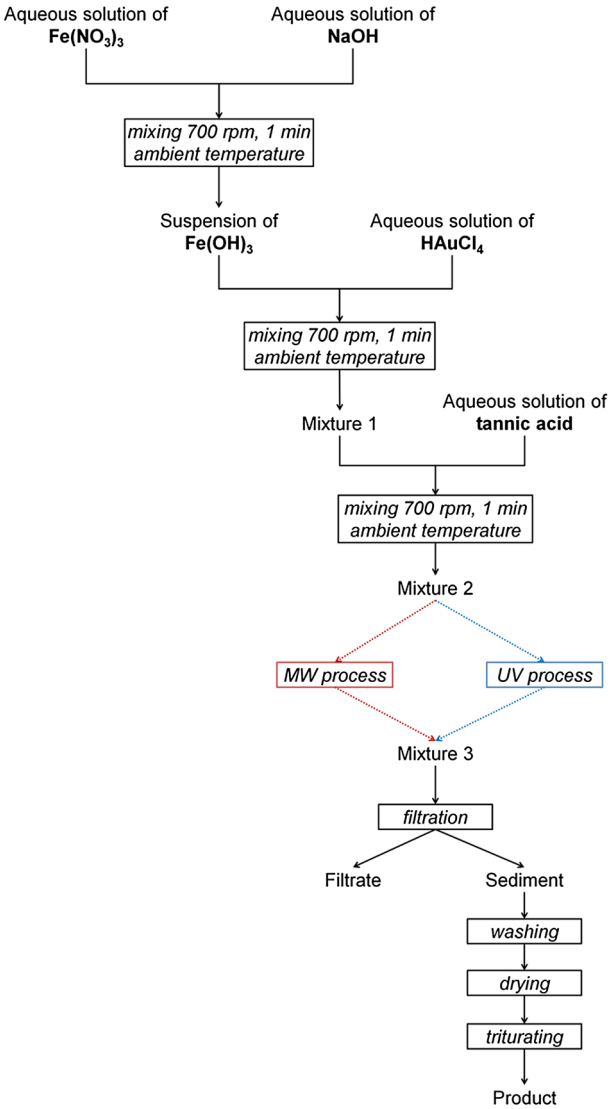

Fig. 1 Schematic diagram of processes

concentration of 0.5 mol/dm^3. The process ran in a glass beaker at room temperature under continuous stirring. Sodium hydroxide was used in a stoichiometric amount.

It was assumed that the incorporation of gold nanoparticles in the structure of iron oxide will occur while gold nanoparticles will be formed in-situ, when the dehydration of iron hydroxide will take place. Gold nanoparticles were obtained using a substance that is characterized by its reducing and stabilizing properties. For this purpose tannic acid was used. Gold(III) chloride served as a source of gold ions. 9.0 cm^3 of gold(III) chloride aqueous solution of sufficient concentration was added to the previously prepared suspension of iron hydroxide. The mixture was stirred at ambient temperature for 1 min. Under continuous stirring 1 cm^3 of tannic acid aqueous solution at sufficient concentration was added to the prepared mixture. As a result, Mixture 2 was obtained. The concentration of tannic acid was calculated based on the fixed molar ratio of that substance to gold ions, which was equal to 0.2. In the processes of obtaining metal nanoparticles using tannic acid it is necessary to activate its phenolic groups by adding hydroxide ions. In the presented method the role of activator is played by sodium hydroxide, which is already present in the reaction mixture.

In order to complete the processes in the microwave field Mixture 2 was transferred to a Teflon vessel and placed in a MAGNUM II microwave reactor (Ertec, Poland).

In order to complete the processes in UV radiation Mixture 2 was transferred to a container and placed in a Crosslinker ultraviolet CL-1000 reactor (UVP, Canada).

The research was performed based on the design of experiments. In the studies the fractional plan (3^{3-1}) with one central repetition was applied. It was generated in the Statistica® program, which is universal statistical software. The group of independent variables contained the concentration of gold in the obtained product (which was calculated in relation to the theoretical mass of iron oxide), time of process, and the power of the applied microwave field/UV radiation. Process parameters are presented in Table 1.

The obtained Mixture 3 was filtrated. The solid sediment was washed with 20 cm^3 of deionized water and dried in an oven at 60 °C for 24 h. The final solid was triturated in a mortar. Each process was performed three times.

Nanometals dispersed in aqueous medium are characterized by presence of surface electrons which may be and are able to absorb and scatter the light. While solid form of gold just scatter electromagnetic irradiation, its spherical nanoparticles are able to absorb it ($\lambda = 500$–600 nm) [22]. In order to asses if any gold nanoparticles were present in the filtrates, they were analyzed spectrophotometrically (UV–Vis), since nanogold aqueous suspensions exhibit a characteristic peak at around 500 nm of wavelength. The analyses were conducted using a Rayleigh UV1800 spectrophotometer.

Inductively coupled plasma with the optical emission spectrometers technique (ICP-OES) is related to electrons transition between specific energy levels. Due to the fact that each element has a specific state of energy, this technique may serve to quantitative identification of elements which is based on the wavelength of emitted radiation generated during the transition of the atom from higher energy state to a

Table 1 Parameters of processes

Microwave processes						UV processes				
Sample	Independent variables			Actual temperature (°C)	Actual pressure (bar)	Sample	Independent variables			Actual pressure (bar)
	C^{a}_{Au} (%)	Time (min)	Power (%)				C^{a}_{Au} (%)	Time (min)	Power (%)	
MW 1	1	5	50	100	8	UV 1	1	30	50	Atmospheric
MW 2	5	5	75	140	17	UV 2	5	30	75	
MW 3	3	5	100	155	31	UV 3	3	30	100	
MW 4	5	10	50	160	14	UV 4	5	60	50	
MW 5	3	10	75	200	31	UV 5	3	60	75	
MW 6	1	10	100	190	31	UV 6	1	60	100	
MW 7	3	15	50	200	25	UV 7	3	90	50	
MW 8	1	15	75	215	31	UV 8	1	90	75	
MW 9	5	15	100	220	31	UV 9	5	90	100	
MW 10	3	10	75	200	31	UV 10	3	60	75	

[a] In order to obtain 1, 3 and 5% content of gold in the final products, the aqueous solutions of gold(III) chloride at concentrations of 2.85×10^{-3}, 8.72×10^{-3} and 1.48×10^{-2} mol/dm^3 and the aqueous solutions of tannic acid at concentrations of 5.13×10^{-3}, 1.57×10^{-2} and 2.67×10^{-2} mol/dm^3 were used respectively

lower energy state [23]. The concentration of iron and gold in the obtained filtrates was determined by ICP-OES technique. It was performed in order to assess whether any unreacted chemicals were present in the filtrates. The analysis was performed on a Plasm 40 apparatus from Perkin Elmer.

Scanning electron microscopy allows to specify the size, shape and distribution of nano- and microparticles analyzed. Imaging occurs by bombarding the sample surface by electron beam, resulting in the dislocation of electrons from the sample and reflection of incident electrons. The resulting map of dislocated and reflected electrons provides the appearance of the surface [24]. The obtained solid products were analyzed in the course of scanning electron microscopy (SEM) and a determination of the shape of the obtained particles was possible.

Energy dispersive spectroscopy is a technique which is complementary to scanning electron microscopy. In the course of this technique, atoms emit X-ray radiation. Each element has the appropriate radiation intensity, which allows direct identification of elements present in the sample [25]. In the course of energy-dispersive X-ray spectroscopy (EDS) the presence of gold on the surface of iron oxide was confirmed. The study was carried out using a 1430 VP microscope from LEO Electron Microscopy Ltd., equipped with an EDS spectrometer. Additionally, microphotographs of obtained samples were taken using high-resolution transmission electron microscopy technique (HRTEM) with EDS and elemental mapping mode. The study was performed on Tecnai Transmission Electron Microscope, F20 X-Twin, FEI Europe. In order to reveal the crystal structure the samples were subjected to X-ray analysis (XRD) conducted on an X-ray diffractometer X'Pert PW 1752/00 from Philips. Based on the Scherrer formula (Eq. 1), which is provided below, the size of crystallites was also calculated.

$$d = \frac{K\lambda}{\beta \cos \Theta} \tag{1}$$

K—dimensionless shape factor (K = 0.9), λ—X-ray wavelength (nm), β—full width of peak at half maximum, Θ—Bragg angle

Thanks to Fourier transform infrared spectroscopy (FT-IR) it is possible to detect the vibration characteristic for individual functional groups [26]. In order to do so samples were subjected to Fourier transform infrared spectroscopy (FT-IR). For this purpose a Nicolet 380 spectrophotometer from Nicolet was used.

In the study iron oxide obtained according to [27] was used as the reference material.

Assessment of Catalytic Activity

The catalytic activity of the obtained products was assessed based on the degradation of methyl orange in comparison without the catalyst, with bare Fe_2O_3 and with obtained Au/Fe_2O_3 composites as the catalyst. For this purpose, 50 cm^3 of aqueous solution of methyl orange at a concentration of 0.1 mol/dm^3 was mixed with 50 cm^3 of aqueous solution of sodium borohydride at a concentration of 0.04 mol/dm^3. The mixture was stirred in a glass baker at room temperature. It

served as the reference sample. In order to catalyze the degradation process, 100 cm^3 of the above-mentioned solution was stirred with 0.1 g of bare Fe_2O_3 or catalytic composite. At regular intervals, 4 cm^3 of the mixture was taken, filtrated and analyzed spectrophotometrically. The methyl orange concentration was evaluated by the measurement of absorbance at 464 nm of wavelength. The percentage of methyl orange degradation was calculated based on the following formula (Eq. 2):

$$Degr.\% = \frac{A_0 - A_t}{A_0} \times 100 \quad (2)$$

A_0—initial absorbance of methyl orange at $\lambda = 464$ nm, A_t—absorbance of methyl orange after specific time (t).

Results

Gold Nanoparticles Embedded in the Structure of Iron Oxide

Figure 2 presents the results of the spectrophotometric analysis of the obtained filtrates. It also provides the model UV–Vis spectra (a) of the suspension of gold nanoparticles obtained according to our previous studies [28]. A characteristic peak

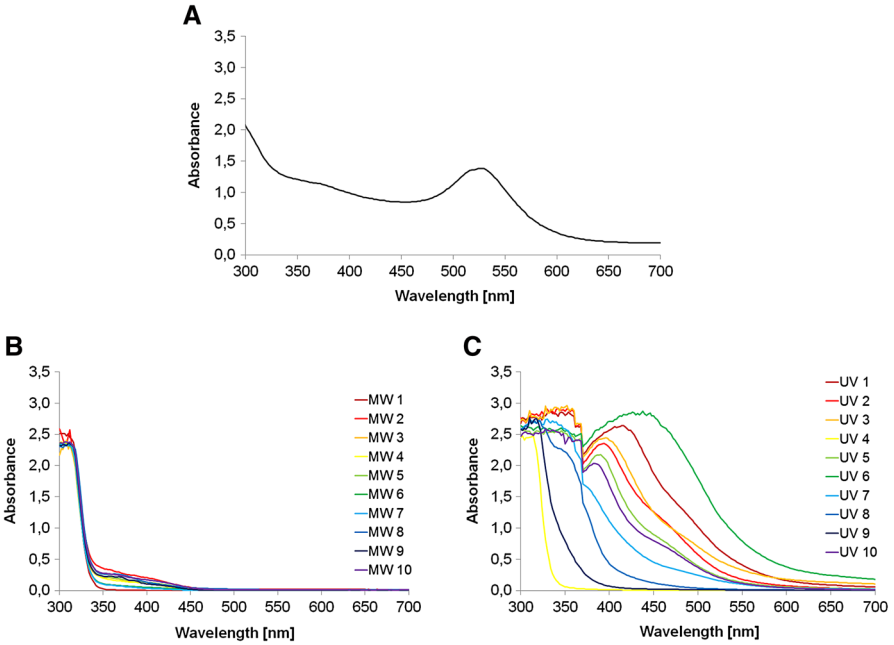

Fig. 2 UV–Vis spectra of gold nanoparticles at a concentration of 100 mg/dm^3 (**a**), filtrates obtained in MW processes (**b**) and filtrates obtained in UV processes (**c**)

originating from the gold nanoparticles can be seen. Its absorbance maximum falls at a wavelength around 500 nm.

Based on the results, it can be concluded that in the case of processes performed in the field of microwave radiation, no gold nanoparticles got to the filtrates. That allows the supposition that all the gold remained in the iron-based matrices. Gold nanoparticles are indicated in some filtrates originating from processes conducted in the field of UV radiation. Peaks that are characteristic of gold nanoparticles occur in the wavelength around 450–500 nm. This means that in these samples gold nanoparticles did not fully bond with iron oxide matrices. Gold nanoparticles are not present only in filtrates of samples UV 4, UV 7, UV 8 and UV 9. These samples were obtained when the lowest power was applied.

Based on the results of the ICP-OES analysis it was possible to calculate the content of gold and iron in filtrates and in solid product. Based on these results the share of these elements present in the product out of the total amount that was introduced into the reaction mixtures was calculated. The obtained results are presented in Table 2.

It can be noticed that in the case of processes that were carried out in the field of microwave radiation, the percentage rate of gold that was indicated in filtrates did not exceed 4%. In general, the higher the values of process time and power were, the less amount of gold was present in filtrates. That means that elongation of time and applying greater power to microwaves enhances better incorporation of gold into the structure of iron oxide matrices. The percentage rate of iron that was indicated in filtrates did not exceed 1%. Overall, the amount of iron that got into the filtrate was not dependent on any input variable.

In the case of processes led in the field of ultraviolet radiation, the values of the percentage rates of gold that did not bind with the iron oxide matrices were much higher than in the case of processes carried out in the microwave reactor. In general, the longer the process time was, the less gold was found in filtrates, and the greater the power was applied, the greater amount of gold was indicated in filtrates. The amount of iron that did not bind with iron oxide matrices was greater when both

Table 2 The percentage rates of gold and iron that were present in iron matrices

Sample	Share (%)[a]		Sample	Share (%)[a]	
	Au	Fe		Au	Fe
MW 1	98.04	99.99	UV 1	99.73	100
MW 2	99.95	99.96	UV 2	71.83	100
MW 3	99.96	99.99	UV 3	95	99.97
MW 4	99.99	99.87	UV 4	99.97	100
MW 5	99.97	99.46	UV 5	39.57	100
MW 6	99.99	99.98	UV 6	3.12	99.94
MW 7	99.89	99.99	UV 7	99.93	100
MW 8	99.63	99.99	UV 8	99.48	100
MW 9	99.96	99.99	UV 9	99.98	98.61
MW 10	96.44	100	UV 10	99.97	100

[a] The calculated share of gold and iron that were present in the product out of total amount of these elements that was introduced into the reaction mixture

time and UV power values were greater. The amount of iron in filtrates was low and constant.

Based on the obtained results, one may conclude that processes led in the field of microwave radiation led to the achievement of a better yield of embedding gold into the structure of iron oxide matrices. The worse results obtained for processes performed in the UV reactor may be due to the fact that UV radiation degrades the crystal structure of iron oxide and bonds between gold and iron oxide. UV radiation may also break the structure of tannic acid, which has reducing properties [29]. It was assumed that the formation of gold nanoparticles will occur in the field of UV radiation. When the structure of tannic acid is damaged, it is difficult to reduce gold ions efficiently, and they may stay in the filtrate. What is more, tannic acid has an extensive spatial structure. Thanks to this structure, it is possible to bind gold nanoparticles with the surface of iron oxide. If its structure is broken, gold may stay in the aqueous suspension and get into the filtrate easily.

Results of XRD analysis are presented in Fig. 3.

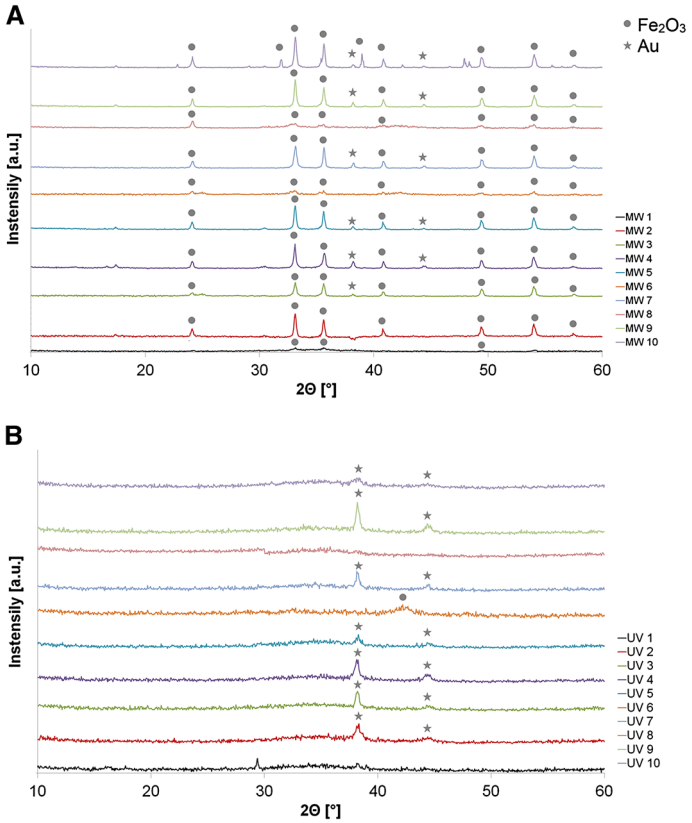

Fig. 3 XRD diffractogram of all samples

The resulting diffractograms differ for both kinds of product. Excluding the sample MW 1, composites obtained in the field of microwave radiation had a crystal structure characterized by a trigonal system. The product named MW 1 had an amorphous structure, which was due to preparing it at insufficient levels of temperature and pressure. Elongation of time and increase of microwave power would result in higher temperature and pressure that would have allowed the building of the crystal structure. Diffractograms obtained for microwave-prepared products exhibit characteristic peaks that indicate the presence of iron oxide and metallic gold. Peaks occurring in the area of 24.20°, 33.18°, 35.75°, 39.41°, 40.95°, 43.61°, 49.52°, 54.08°, 56.35° and 57.76° of 2θ diffraction angle correspond to strong Bragg reflection originating from α-Fe_2O_3 (JCPDS card No. 73-603). Peaks occurring in the area of 38.27° and 44.51° of 2θ diffraction angle indicate metallic gold (JCPDS card No. 1-1172). Peak intensity (excepting MW 1 and MW 8) provides high crystallinity of products, and their width reflects the small size of crystallites.

Other reflections were not detected, which indicates the high purity of samples.

In the case of products obtained in the field of ultraviolet radiation, all samples had an amorphous structure. That was due to the fact that temperature-pressure conditions were inadequate for obtaining crystal iron oxide. Since low values of UV-process parameters did not enable obtaining highly crystalline metal oxide, the detection limit of XRD was reduced. That is the reason of amorphous structure which was predominantly detected. Nevertheless, peaks characteristic for metallic gold are noticeable in the diffractograms. In the case of samples UV 1, UV 6, UV 8 and UV 10 reflections from gold are hardly seen. This complies with the results obtained in the course of the spectrophotometric analysis of filtrates. That means that in these samples gold did not embed in the iron matrices.

Values of calculated crystallites size are given in Table 3.

It can be noted that these size values concern the size of individual iron oxide crystallites, which may consist of the structure of nanoparticles that are characterized by larger sizes.

Table 3 Crystallites size calculated based on Scherrer equation

Sample	d_{mean} (nm)	Crystal system
Ref.	38	Trigonal (hexagonal axes)
MW 1	Amorphous	
MW 2	33	Trigonal (hexagonal axes)
MW 3	31	
MW 4	37	
MW 5	35	
MW 6	12	
MW 7	31	
MW 8	10	
MW 9	39	
MW 10	37	

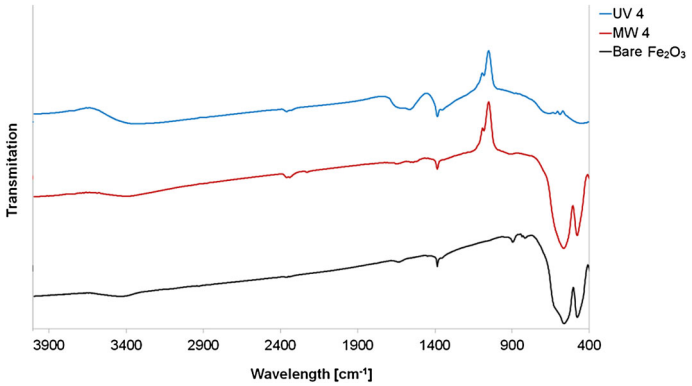

Fig. 4 FTIR spectra of obtained nanocomposites

Figure 4 presents the results of FT-IR analysis of pure iron oxide and modified with gold nanoparticles (samples MW 4 and UV 4).

In the case of bare Fe_2O_3 and nanoAu/Fe_2O_3 obtained in the field of microwave radiation (sample MW 4), two prominent absorption peaks occur in the region below 700 cm^{-1}. They appear at around 475 and 550 cm^{-1} and originate from the metal–oxygen (Fe–O) vibrations, which is in good accordance with literature data [30, 31]. The poorly developed band at 1400 cm^{-1} may be attributed to –OH bending vibrations combined with Fe atoms. This may be due to the presence of an unreacted $Fe(OH)_3$ remnant. When it comes to results for the UV 4 sample, there is a lack of strong peaks below 700 cm^{-1}. That means that conditions in the UV reactor were not sufficient to perform the $Fe(OH)_3$ dehydration process completely, and no Fe_2O_3 reflections were identified. What is more, the peak at around 700 cm^{-1} indicates the presence of Fe–OH vibration modes, which confirms the thesis that the sample consisted mainly of $Fe(OH)_3$ matrices. The weak peaks at around 2350 cm^{-1} that occur in spectra obtained for samples MW 4 and UV 4 are related to the O–H stretching vibrations that originate from tannic acid molecules. This indirectly confirms the presence of gold nanoparticles in the samples.

Results of SEM-EDS analysis are provided in Figs. 5 and 6.

In all cases the presence of gold on the iron oxide matrices was confirmed. The greater theoretical concentration of gold in samples is visible on the obtained microphotographs. Gold nanoparticles have a spherical shape. Their size distribution is homogeneous. It can be seen that the arrangement of gold nanoparticles on the iron oxide surface is regular.

TEM images of obtained nanoAu/Fe_2O_3 composites are presented in Fig. 7.

Results confirm the creation of nanocomposites that are consisted of gold particles on iron oxide matrix. Both gold and iron oxide particles are spherical. Iron oxide matrix that is presented in Fig. 7a (sample obtained in the field of microwave radiation) seems to be more crystalline than iron oxide shown obtained in ultraviolet radiation. This fact agrees with data obtained in XRD analysis.

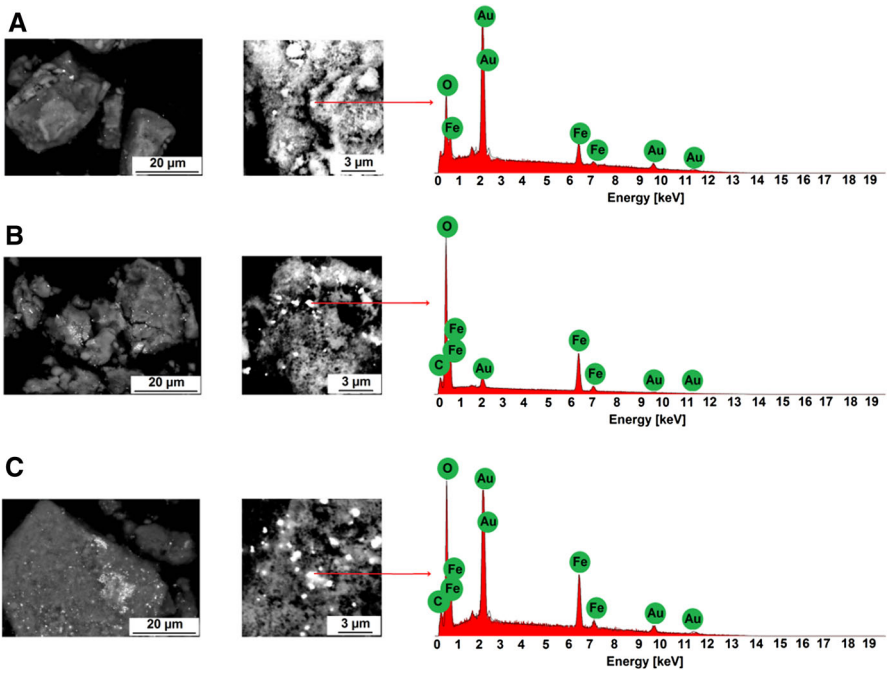

Fig. 5 SEM microphotographs and EDS collective spectrum of nanocomposites obtained in the field of microwave radiation: **a** sample MW 8 ($C_{Au} = 1\%$), **b** sample MW 7 ($C_{Au} = 3\%$), **c** sample MW 4 ($C_{Au} = 5\%$)

Catalytic Activity

The catalytic activity of the obtained composites was evaluated based on the degradation process of methyl orange when using sodium borohydride. The degradation of methyl orange without any catalyst and when using bare Fe_2O_3, as well as selected composites, was evaluated in time. Figure 8 presents the results of catalytic activity studies.

It can be noted that the faster degradation of methyl orange occurred when catalysts obtained in the field of microwave radiation were used. It was possible to degrade methyl orange to around 90% even after 2 min (MW 7 and MW 4). In the case of using catalysts obtained in the field of ultraviolet radiation, a similar degradation rate was achieved only when using the composite with the highest concentration of gold nanoparticles. Lower Au content allowed the achieving of similar results in a longer time (around 7 min). It is clearly seen that the higher the concentration of gold nanoparticles, the greater the degradation rate obtained. The worse results obtained for samples prepared in UV radiation are due to the actual lower concentration of gold. This method did not allow the full incorporation of nanogold into the iron oxide matrices, which was confirmed in previously reported studies' results. It is interesting that using bare Fe_2O_3 gave the worst results. It inhibits the process of methyl orange degradation.

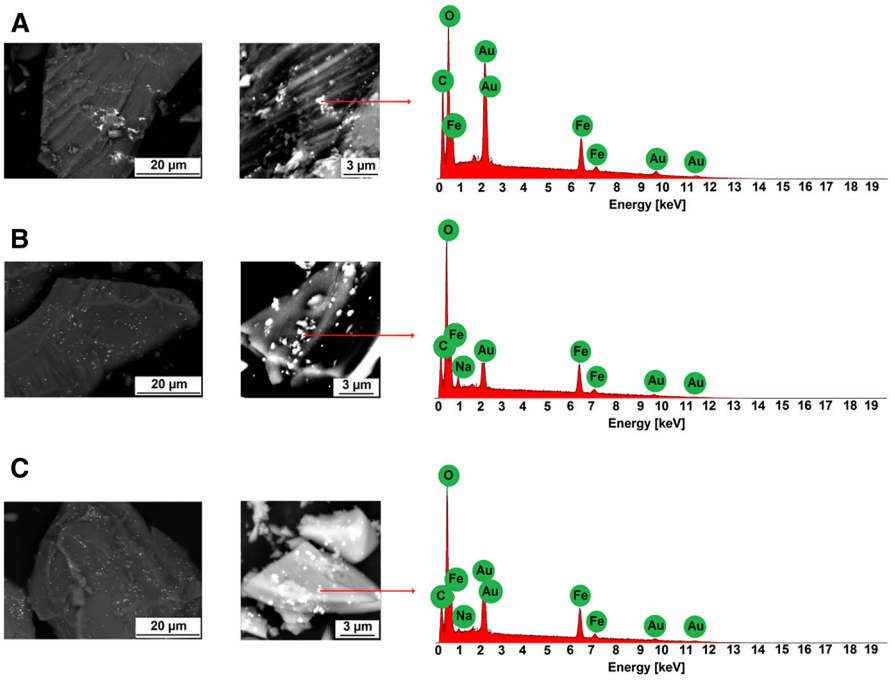

Fig. 6 SEM microphotographs and EDS collective spectrum of nanocomposites obtained in the field of UV radiation: **a** sample UV 8 ($C_{Au} = 1\%$), **b** sample UV 7 ($C_{Au} = 3\%$), **c** sample UV 4 ($C_{Au} = 5\%$)

Discussion

It is worth noting that applying tannic acid ensures the total reduction of gold ions and the effective stabilization of the formed gold nanoparticles. The mechanism of action of tannic acid in processes for obtaining metal nanoparticles is as presented below (Fig. 9).

Tannic acid is a derivative of gallic acid. It belongs to the group of polyphenols. Its molecule is a combination of glucose with ten molecules of gallic acid. The value of the tannic acid dissociation constant ($pK_a = 5.12$) suggests that this is a weak acid. Its structure includes numerous hydroxyl groups. Thanks to them, tannic acid can successfully be used as an antioxidant or as a reducing substance. It is able to capture reactive unpaired electrons in the oxygen radicals [33, 34].

Similarly, tannic acid can provide electrons in the reduction of metal ions, transferring them to the zero oxidation state. Tannic acid is able to detach the hydrogen atom from the carboxyl group and to give electrons to reduce ions into a metallic form. That leads to the formation of carbanions by which the molecule can bind to the nanoparticle surface. This kind of stabilization is named "electrosteric stabilization". Thanks to that, the attraction of the nanoparticles is hindered by the presence of side chains. The tannic acid molecule has an extensive spatial structure, so that it also represents a spatial factor preventing agglomeration of the particles. Thus, the stability of the colloidal system is conditioned by the rise of molecular

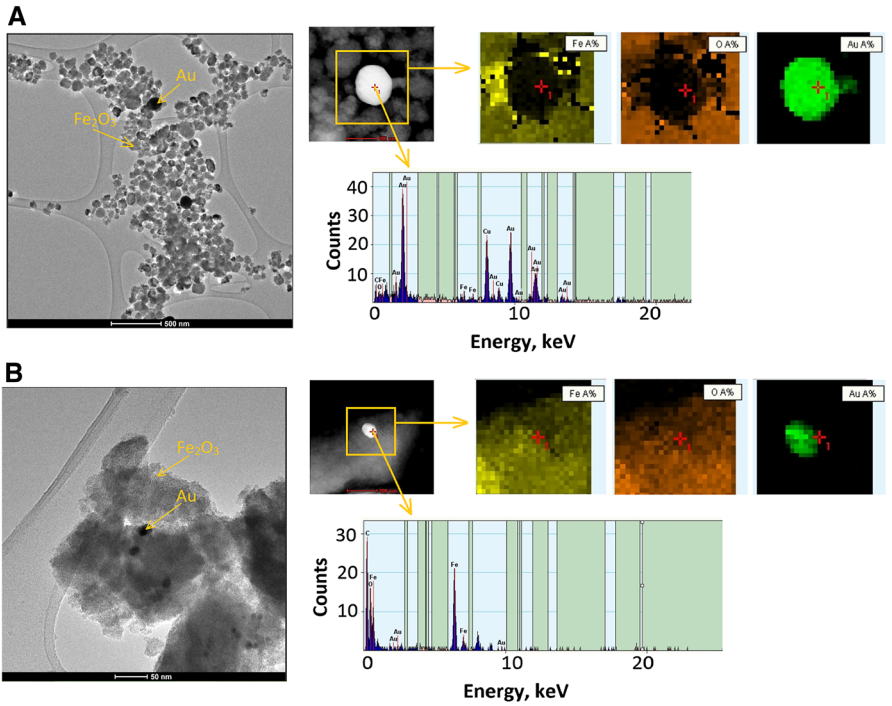

Fig. 7 TEM images, EDS collective spectrum and mapping of obtained nanocomposites (**a** MW 4, **b** UV 4)

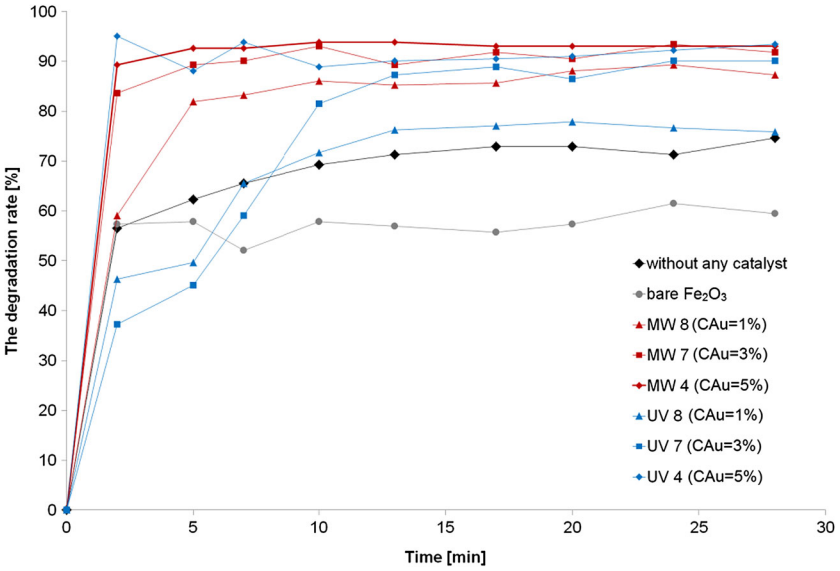

Fig. 8 Results of degradation process of methyl orange when using catalysts and without any catalyst

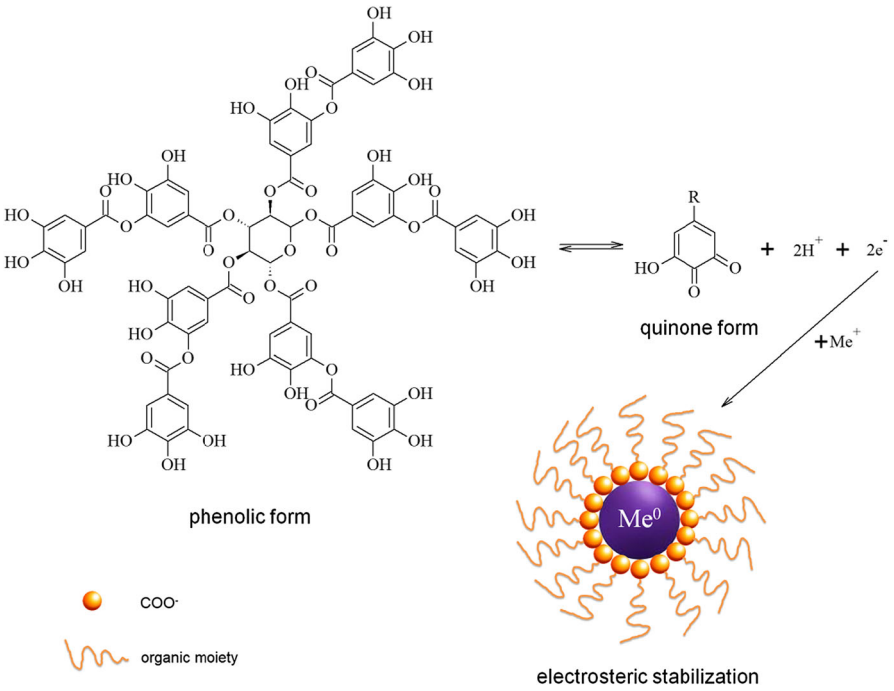

Fig. 9 Mechanism of reduction of metal ions with tannic acid [32]

anions of tannic acid and their adsorption on the surface of metallic nanoparticles [35, 36].

Processes of dehydration of iron hydroxide and reduction of gold ions carried out in the field of microwave and ultraviolet radiation were varied through the selection of different conditions. In fact, specific values of radiation power and the residence time determined the temperature and, in the case of the microwave reactor, also the pressure of the performed processes. In the case of processes that were carried out in the field of microwave radiation, thanks to the use of polar solvent (water) it was possible to enhance the efficiency of heat transfer. In a shorter time the whole volume of the reaction mixture is heated, which accelerates the process of iron hydroxide dehydration and the process of gold ions reduction. Performing processes in presented way reflects the rules of green chemistry and cleaner technologies. Similar studies were performed by Mishra et al. [37]. They obtained nanoAu/Fe_2O_3 composite based on co-precipitation method. After the precipitate was formed, it must have been calcined at 400 °C for 4 h. In our work, the longest time of processes conducted according to UV method was equal to 90 min and according to MW method—barely 15 min. Any additional time which would be essential for obtaining crystalline product was unnecessary. From the technological point of view, this feature makes the process more profitable. Also, Gunawan et al conducted similar researches [38]. In their work, Au or Pt nanoparticles were incorporated in the structure of α-Fe_2O_3. Firstly, tetraethylammonium hydroxide (TEAOH) served

to precipitate goethite (FeOOOH). After that, the precipitate was subjected to microwave irradiation and next the product was calcined. It was followed by sonication process in which previously obtained Fe_2O_3 was mixed with gold or platinum precursor, capping agent and reducing agent (sodium borohydrate). Using organic compound (TEAOH) does not allow treating this method as environment friendly. What is more, sodium borohydrate is not a safe chemical since in contact with the skin it releases flammable gases and causes burns. Moreover, the referenced method is multi-step one, while in our method gold nanoparticles were formed in-situ—in the process of Fe_2O_3 formation. In the work of Ayastuy et al. [39] it was possible to obtain Au/Fe_2O_3 composite in the course of two-step method. Firstly, iron nitrate was treated with sodium carbonate. The prepared solid was filtrated, washed, dried and calcined. Deposition of gold particles on the Fe_2O_3 surface occurred by mixing previously obtained iron oxide suspension with chloroauric acid and urea. The obtained slurry was filtrated, washed, dried and calcined. Taking into consideration the technological aspects, the multiplicity of process steps does not make this method efficient enough.

The process of the degradation of methyl orange occurs according to the following chemical Eqs. (3, 4) [40].

$$BH_4^- + 3H_2O \rightarrow BO_3^{3-} + 8e^- + 10H^+ \tag{3}$$

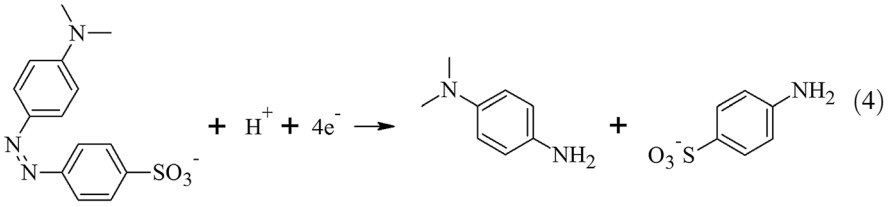

(4)

The speculated mechanism of the catalytic activity of obtained nanocomposites is presented in Fig. 10.

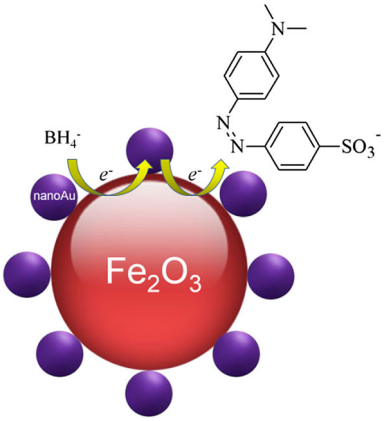

Fig. 10 Speculated mechanism of the catalytic activity of nanoAu/Fe_2O_3 nanocomposites [40]

Gold nanoparticles act as the centrum of electron transfer. Firstly, borohydride ions and methyl orange migrate to gold nanoparticles. In the second step, nanoAu accepts electrons from borohydride ions. Next, they pass them to methyl orange particles. As a result, borohydride ions are oxidized to borate ions. Reduced methyl orange forms amine organic compounds. This catalytic activity may refer to other processes in which metals deposited on metal oxide surfaces are used as catalysts.

Conclusions

It was possible to obtain nanogold incorporated into the structure of iron oxide particles by applying fields of both microwave and ultraviolet radiation. Nevertheless, the processes were performed with greater effectiveness when using microwave radiation. What is more, this kind of method allowed the significant reduction of the process time. The desired products were obtained even after 5 min. The prepared nanocomposites can be applied as catalysts in various processes in which metal on metal oxide is used as a catalyzing substance. Composites with a greater amount of gold are characterized by better catalytic activity.

Acknowledgements This research did not receive any specific grant from funding agencies in the public, commercial, or not-for-profit sectors.

References

1. N. S. Bijlania and S. B. Chandalia (1981). *Indian Chem. Eng.* **23**, 44.
2. L. F. Liotta, A. M. Venezia, G. Deganello, A. Longo, A. Martorana, Z. Schay, and L. Guczi (2001). *Catal. Today* **66**, 271.
3. I. Matsushita, K. Ebitani, and K. Kaneda (1999). *Chem. Commun.* **9**, 265–266.
4. V. R. Choudhary and D. K. Dumbre (2009). *Catal. Commun.* **10**, 1738.
5. A. Luengnaruemitchai, S. Osuwana, and E. Gulari (2004). *Int. J. Hydrogen Energy* **29**, 429.
6. S. N. Rashkeev, A. R. Lupini, S. H. Overbury, S. J. Pennycook, and S. T. Pantelides (2007). *Phys. Rev. B* **76**, 035438.
7. X. Zhou, W. Xu, G. Liu, D. Panda, and P. Chen (2010). *J. Am. Chem. Soc.* **132**, 138.
8. B. V. Reddy, F. Rasouli, M. R. Hajaligol, and S. N. Khann (2004). *Chem. Phys. Lett.* **384**, 242.
9. N. Perkas, Y. Q. Wang, Y. Koltypin, A. Gedanken, and S. Chandrasekaran (2001). *Chem. Commun.* **11**, 988.
10. J. S. K. Teo, S. P. Teh, W. P. Addiego, Z. Zhong, A. Borgna, and R. E. Truitt (2011). *Int. J. Hydrogen Energy* **36**, 5763.
11. C. Feldmann (2001). *Advanced Materials* **13**, 1301.
12. Z. Y. Wang, D. Y. Luan, S. Madhavi, C. M. Li, and X. W. Lou (2011). *Chem. Commun.* **47**, 8061.
13. Q. Hao, S. Liu, X. Yin, Z. Du, M. Zhang, L. Li, Y. Wang, T. Wang, and Q. Li (2011). *CrystEngComm* **13**, 1466.
14. K. Woo, H. J. Lee, J. P. Ahn, and Y. S. Park (2003). *Adv. Mater.* **15**, 176.

15. C. J. Jia, L. D. Sun, Z. G. Yan, L. P. You, F. Luo, X. D. Han, Y. C. Pang, Z. Zhang, and C. H. Yan (2005). *Angew. Chem.* **44**, 4328.
16. M. Date, Y. Y. Ichihashi, T. Yamashita, A. Chiorino, F. Boccuzzi, and M. Haruta (2002). *Catal. Today* **72**, 89.
17. S. Lee, A. Gavriilidis, Q. A. Pankhurst, A. Kyek, F. E. Wagner, P. C. L. Wong, and K. L. Yeung (2001). *J. Catal.* **200**, 298.
18. J. E. Bailie, H. A. Abdullah, J. A. Anderson, C. H. Rochester, N. V. Richardson, N. Hodge, J.-G. Zhang, A. Burrows, C. J. Kiely, and G. J. Hutchings (2001). *Phys. Chem. Chem. Phys.* **3**, 4113.
19. M. Khoudiakov, M. C. Gupta, and S. Deevi (2005). *Appl. Catal. A: Gen.* **291**, 151.
20. R. Liu, C. Zhang, and J. Ma (2010). *Chem. Res. Chin. Univ.* **26**, 98.
21. T. T. M. Nguyet, N. C. Trang, N. Q. Huan, and N. Xuan (2008). *J. Korean Phys. Soc.* **52**, 1345.
22. K. Lu *Nanoparticulate Materials. Synthesis, Characterization, and Processing* (Willey, New Jersey, 2013).
23. M. Kozak (2010). Zastosowanie optycznej spektrometrii emisyjnej, ze wzbudzeniem w plazmie indukowanej w badaniach przetworów naftowych. *Nafta-Gaz* **7**, 606–612.
24. M. Oćwieja, M. Morga, and Z. Adamczyk (2013). Self-assembled silver nanoparticles monolayers on mica-AFM, SEM, and electrokinetic characteristics. *J. Nanopart. Res.* **15**, 1460–1475.
25. T. C. Lovejoy, Q. M. Ramasse, M. Falke, A. Kaeppel, R. Terborg, R. Zan, N. Dellby, and O. L. Krivanek (2012). Single atom identification by energy dispersive X-ray spectroscopy. *Appl. Phys. Lett.* **100**, 154101-1–154101-4.
26. P. Griffiths and J. A. de Hasseth *Fourier Transform Infrared Spectrometry* (Wiley-Blackwell, New Jersey, 2007).
27. M. Banach, and J. Pulit (2013). Patent Application P.405172.
28. M. Banach, and J. Pulit (2013). Patent Application P.404952.
29. R. Cruz, L. H. Reyes, J. L. Guzman-Mar, J. M. Peralta-Hernandez, and A. Hernandez-Ramirez (2011). *Sustain. Environ. Res.* **21**, 307.
30. M. R. Belkhedkar and A. U. Ubale (2014). *Int. J. Mater. Chem.* **4**, 109.
31. S. Zhan, D. Chen, X. Jiao, and S. Liu (2007). *J. Colloid Interface Sci.* **308**, 265.
32. T. Ahmad (2014). *J. Nanotechnol.* Article ID 954206.
33. İ. Gülçina, Z. Huyutb, M. Elmastaşc, and H. Y. Aboul-Enein (2010). *Arab. J. Chem.* **3**, 43.
34. R. G. Andrade, L. T. Dalvi, J. N. Silva, G. K. Lopes, A. Alonso, and M. Hermes-Lima (2005). *Arch. Biochem. Biophys.* **1**, 1.
35. A.R. Senoudi, S.M.C. Sari, and I.F. Hakem (2014). *Int. J. Anal. Chem.* Article ID 832657.
36. D. Lin and B. Xing (2008). *Environ. Sci. Technol.* **42**, 5917.
37. M. Mishra, H. Park, and D. M. Chun (2016). *Adv. Powder Technol.* **27**, 130.
38. P. Gunawan, L. Mei, J. Teo, J. Ma, J. Highfield, Q. Li, and Z. Zhong (2012). *Langmuir* **28**, 14090.
39. J. L. Ayastuy, A. Gurbani, and M. A. Gutierrez-Ortiz (2016). *Int. J. Hydrogen Energy* **41**, 19546.
40. X. L. Liu, X. Yang, H. Y. Xin, P. Tang, L. J. Weng, Y. Y. Han, and D. Geng (2016). *Dig. J. Nanomater. Biostruct.* **11**, 337.